To appear in The Astrophysical Journal
Preprint typeset using LaTeX style emulateapj v. 14/09/00

arXiv:astro-ph/0204102v1 5 Apr 2002

VARIABILITY IN THE THERMAL EMISSION FROM ACCRETING NEUTRON STAR TRANSIENTS

Edward F. Brown
University of Chicago, Enrico Fermi Institute, 5640 S. Ellis Ave, Chicago, IL 60637
brown@flash.uchicago.edu
Lars Bildsten
Institute for Theoretical Physics and Department of Physics, Kohn Hall, University of California, Santa Barbara, CA 93106
bildsten@itp.ucsb.edu
and
Philip Chang
Department of Physics, Broida Hall, University of California, Santa Barbara, CA 93106
pchang@physics.ucsb.edu
Final version 3 April 2002

ABSTRACT

The composition of the outer 100 m of a neutron star sets the heat flux that flows outwards from the core. For an accreting neutron star in an X-ray transient, the *thermal* quiescent flux depends sensitively on the amount of hydrogen and helium remaining on the surface after an accretion outburst and on the composition of the underlying ashes of previous H/^{4}He burning. Because H/^{4}He has a higher thermal conductivity, a larger mass of H/^{4}He implies a shallower thermal gradient through the low density envelope and hence a higher effective temperature for a given core temperature. The mass of residual H and ^{4}He varies from outburst to outburst, so the thermal quiescent flux is variable even though the core temperature is constant for timescales $\lesssim 10^4$ yr. Heavy elements settle from a H/^{4}He envelope in a few hours; we therefore model the quiescent envelope as two distinct layers, H/^{4}He over heavier elements, and treat the mass of H/^{4}He as a free parameter. We find that the emergent thermal quiescent flux can vary by a factor of 2 to 3 between different quiescent epochs. The variation is more pronounced at lower interior temperatures, making systems with low quiescent luminosities and frequent outbursts, such as SAX J1808.4−3658, ideal candidates from which to observe this effect. Because the ashes of H/^{4}He burning are heavier than ^{56}Fe, their thermal conductivity is greatly reduced. This increases the inferred crust temperature beyond previous estimates for a given effective temperature. We survey this effect for different ash compositions and apply our calculations to Cen X-4, Aql X-1, and SAX J1808.4−3658. In the case of Aql X-1, the inferred high interior temperature suggests that neutrino cooling contributes to the neutron star's thermal balance.

Subject headings: conduction—diffusion—stars: individual (Aql X-1, Cen X-4, SAX J1808.4−3658)—stars: neutron—X-rays: binaries

1. INTRODUCTION

The orbiting X-ray observatories *Chandra* and *XMM* have dramatically improved our understanding of soft X-ray transients (SXTs): binaries containing a neutron star or black hole primary and having well-defined accretion outbursts separated by long periods of quiescence. These objects are typically defined as having a ratio of outburst flux to quiescent flux > 1000. Two puzzles are pertinent to this work. The first is whether the thermal component of the neutron star's quiescent luminosity is powered by accretion or by thermal emission from the cooling core. This has implications for the observed contrast in the quiescent luminosity between transient black holes and neutron stars (Narayan et al. 1997; Menou et al. 1999; Garcia et al. 2001; Kong et al. 2002).

Brown et al. (1998) showed that compression-induced reactions—electron captures, neutron emissions, and pycnonuclear reactions (Bisnovatyi-Kogan & Chechetkin 1979; Sato 1979; Haensel & Zdunik 1990)—in the inner crust of an accreting neutron star release enough heat to power a cooling luminosity of order 10^{33} ergs s^{-1} in quiescence. In the absence of neutrino emission from the core the quiescent thermal flux is proportional to the mean outburst flux (Brown et al. 1998; Colpi et al. 2001). Motivated by the match between the expected quiescent luminosity and that observed from neutron star SXT's in quiescence, Rutledge et al. (1999, 2000) fit archival *ROSAT* and *ASCA* observations of Aql X-1, Cen X-4, 4U 1608−522, and 4U 2129+47 with realistic H (or ^{4}He) atmosphere spectra and found that the emission could be explained as thermal emission from an area of radius ≈ 10 km. Further *Chandra* observations of Cen X-4 (Rutledge et al. 2001b), Aql X-1 (Rutledge et al. 2001a), and KS 1731−260 (Wijnands et al. 2001; Rutledge et al. 2001c), as well as quiescent transient neutron star identifications in ω Cen (Rutledge et al. 2002b), NGC 6440 (Pooley et al. 2002), and 47 Tuc X5 and X7 (Heinke et al. 2002) confirm that the quiescent spectra of neutron star transients is consistent with being thermal emission (effective temperature $k_{\rm B}T_{\rm eff} \gtrsim 100$ eV) from a H photosphere, plus, in most cases, an additional hard power-law component. The ori-

gin of the power-law tail remains uncertain (for a review of proposed mechanisms, see Campana et al. 1998; also see Menou & McClintock 2001).

The second puzzle is the source of the observed variability in the quiescent emission on timescales > 1 d. Indeed, it was in part because of an apparent *increase* in the quiescent intensity of Cen X-4 between 1980 (*EINSTEIN*) and 1984 (*EXOSAT*) that led van Paradijs et al. (1987) to discount the possibility that the observed emission was intrinsic to the neutron star, i.e., not powered by accretion. *ROSAT*/HRI observations of Cen X-4 (Campana et al. 1997) revealed that the intensity decreased by a factor of ≈ 3 over 4 days. Similarly, there was a fractional decrease of 40 % in the observed intensity between an *ASCA* observation and one 5 yr later with *Chandra*, although this could be attributed to variability in the power-law component only (Rutledge et al. 2001b). A comparison of Aql X-1 observations taken with *Chandra*/ACIS-S, *ROSAT*/PSPC, and *ASCA* (Rutledge et al. 2001a) indicates variability by a factor of 2 over a timescale of roughly 8 yr. Note that in this case there were several intervening outbursts between the different observations. In both cases, there was no short-timescale ($\lesssim 10^4$ s) variability detected (Rutledge et al. 2001b,a). More recently, Rutledge et al. (2002a) used the *Chandra*/ACIS-S to take four "snapshots" of Aql X-1 after a recent outburst. The intensity was observed to decrease by a factor ≈ 0.5 over 3 months and then increase by a factor ≈ 1.4 over 1 month. In addition, short-timescale variability was found in the last observation.

The standard interpretation is that the observed variability is caused by fluctuations in the quiescent accretion rate (van Paradijs et al. 1987; Campana et al. 1997; Brown et al. 1998; Rutledge et al. 2001b,a; Menou & McClintock 2001; Dubus et al. 2001). In this manuscript, we describe a previously overlooked cause of variability in the intrinsic quiescent thermal emission: a changing envelope[1] composition. Even if accretion completely halts in quiescence, the neutron star's envelope will have a different stratification following each outburst. This varying composition can change the quiescent flux by a factor of 2 to 3 for a fixed crust/core temperature.

Previous calculations of the thermal structure of a cooling unmagnetized neutron star considered the difference between a purely ^{56}Fe envelope (Gudmundsson et al. 1983) and one composed of light elements (H, ^{4}He, and ^{12}C) overlying ^{56}Fe (Potekhin et al. 1997). Consider two hypothetical neutron stars each with a core/crust temperature of $T_{\rm b} = 10^8$ K (typical of neutron star SXT's; see below); one star has a pure ^{56}Fe envelope and the other has H and ^{4}He at densities $< 10^5$ g cm^{-3}. As noticed by Potekhin et al. (1997), the large difference in opacity between a pure iron and a light element envelope means that the effective temperature, $T_{\rm eff}$, for the light element envelope is a factor of 1.6 hotter: $T_{\rm eff}(^{56}{\rm Fe}) = 1.1 \times 10^6$ K and $T_{\rm eff}({\rm light\ element}) = 1.8 \times 10^6$ K. Gudmundsson et al. (1983) first noticed that the thermal stratification is sensitive to the opacity in the region where the electrons are semi-degenerate. Coincidentally, it is in this region that the accreted H and ^{4}He unstably ignite. As a result the thermal gradient through the envelope depends on the mass of H and ^{4}He remaining after the *previous* accretion outburst. Our calculation thus addresses variations in the quiescent flux from one quiescent epoch to the next, as the intervening outburst changes the composition and mass of the outermost layers of the neutron star. Changes in the quiescent intensity over a timescale of months can also occur from differential sedimentation of ions and residual accretion. Neither of these scenarios can explain short timescale ($< 10^4$ s) variability such as just observed from Aql X-1 (Rutledge et al. 2002a).

This paper first (§ 2) describes in qualitative terms the overall stratification of a quiescent neutron star transient. Section 3 contains a summary of the relevant microphysics in the calculation: the equation of state (EOS), diffusive sedimentation of ions, and thermal transport. In § 4 we describe how changing the composition and stratification of the envelope produces variations in the surface effective temperature. This calculation is then applied, in § 5, to Aql X-1, Cen X-4, and SAX J1808.4−3658. Implications and directions for future study are discussed in § 6.

2. THE COMPOSITION AND STRATIFICATION OF QUIESCENT NEUTRON STAR ENVELOPES

In the absence of accretion, the thermal structure of the envelope is determined, over durations much less than the cooling timescale of the core (i.e., $\lesssim 10^4$ yr), by the flux equation

$$\frac{\mathrm{d}}{\mathrm{d}y}\left(\frac{T}{T_{\rm eff}}\right)^4 = \frac{3}{4}\kappa. \qquad (1)$$

Here $\kappa = (\kappa_{\rm r}^{-1} + \kappa_{\rm c}^{-1})^{-1}$ is the reciprocal sum of the radiative opacity $\kappa_{\rm r}$ and the conductive opacity $\kappa_{\rm c}$,

$$\kappa_{\rm c} = \frac{16\sigma_{\rm R}T^3}{3\rho K}, \qquad (2)$$

with K and ρ being the electron thermal conductivity and mass density. The spatial coordinate is just the column depth, $y = \int_r^\infty \rho\,\mathrm{d}r = p/g$ by hydrostatic balance. We use the Newtonian form of the thermal diffusion equation: the thickness of the envelope is much less than the stellar radius, so that the gravitational redshift $1 + z \approx [1 - 2GM/(Rc^2)]^{-1/2}$ is nearly constant across the envelope and factors from equation (1). All quantities in this manuscript refer to proper quantities; in particular the effective temperature as observed far away from the star is $T_{\rm eff,\infty} = T_{\rm eff}(1+z)^{-1}$.

For a fixed envelope stratification, the flux equation (1) guarantees a one-to-one mapping between $T_{\rm b}$ and $T_{\rm eff}$. The core temperature cannot change on timescales $\ll 10^4$ yr, so if the envelope composition were constant, then the basal effective temperature and luminosity would be unchanging from quiescent epoch to quiescent epoch. For an accreting neutron star the envelope composition and stratification are not, however, fixed. During each outburst, H and ^{4}He are deposited onto the surface of the neutron star. After accumulation of a critical column

[1] In this paper "envelope" means the outermost layer of the neutron star where the thermal gradient is significant. This is distinct from the photosphere, where the emergent continuum spectrum forms.

$y_{\rm ign} \sim 10^8$ g cm^{-2}, the H and ^{4}He burn to heavier elements ("ashes"), and the process then repeats. As the outburst wanes, there is a last episode of unstable burning (a type I X-ray burst). Accretion after this last type I burst deposits a residual H/^{4}He layer of column $y_{\rm i} < y_{\rm ign}$ onto the ashes of previous episodes of H/^{4}He burning. The depth of the light element layer is effectively unconstrained, and as a result $T_{\rm eff}$ can vary even though $T_{\rm b}$ is fixed.

The composition of the ashes depends on the nature of the H/^{4}He burning (for a recent review, see Bildsten 2000); for most accretion rates, the ^{4}He unstably ignites in the presence of H. The H is then consumed by the rp-process, a sequence of rapid proton captures onto seeds provided by the ^{4}He burning (Wallace & Woosley 1981; Van Wormer et al. 1994; Schatz et al. 1998). Reaction network calculations, both for single-zone calculations of unstable burning (Koike et al. 1999; Schatz et al. 2001) and for steady burning (Schatz et al. 1999), find that all of the hydrogen is consumed and that the reactive flow reaches nuclei much heavier than ^{56}Fe. In a recent calculation, Schatz et al. (2001) determined that the rp-process ends in a closed SnSbTe cycle; the resultant ash composition has a mean nuclear charge $\langle Z \rangle = 37$ and a mean nuclear mass $\langle A \rangle = 79$. Following the burst, the proton-rich elements quickly β-decay to more stable species such as ^{104}Ru.

The ratio of H to ^{4}He is not well determined. When the temperature in the crust exceeds roughly 10^8 K, the H in the outer envelope is consumed on a timescale $\approx 6 \times 10^4$ s $(X_{\rm CNO}/0.02)$ by the hot CNO cycle, $X_{\rm CNO}$ being the mass fraction of CNO nuclei. Hydrogen is also consumed (in a thermally stable fashion) when the accretion rate exceeds about $2 \times 10^{-10}\ M_\odot$ yr^{-1}. During the outburst decay, a significant fraction of the accumulated H can be converted stably to ^{4}He, even after the last type I X-ray burst has occurred. We include this possibility in our calculations (§ 4). We note, however, that the photosphere would still tend to be pure H, as $T_{\rm eff}$ is too cold for the H to be consumed on a timescale over which differential sedimentation removes CNO nuclei from the photosphere (~ 10 s; Bildsten et al. 1992). As a result, spectral fitting of the quiescent flux will find that the ratio of radius to distance remains constant even if $T_{\rm eff}$ varies. Changes in the photospheric abundances, as implied by, e.g., spectral features, more likely indicate quiescent accretion.

3. EQUATION OF STATE, SEDIMENTATION, AND THERMAL TRANSPORT

The microphysics of the envelope enters equation (1) explicitly through the opacity κ and implicitly through $\rho(y = p/g, T)$. Before discussing the thermal transport and its effect on the thermal structure of the envelope, we first review the different physical regimes of the neutron star's envelope, the equation of state, and the validity of treating the envelope as being composed of distinct layers. Figure 1 shows different regimes of the ρ–T plane for an envelope composed of a pure H layer, of column depth $y = 10^8$ g cm^{-2}, superincumbent on a ^{104}Ru layer. The top panel illustrates conditions in the H layer; the bottom panel does likewise for the ^{104}Ru layer. In both panels, the circles denote the thermal structure found by solving equation (1) for $T_{\rm eff} = 2.1 \times 10^6$ K (as inferred for Aql X-1; *top curve*) and $T_{\rm eff} = 8.8 \times 10^5$ K (as inferred for Cen X-4; *bottom curve*). We discuss the calculations for these sources in § 5.

3.1. *Equation of State*

The envelope of a neutron star is composed of electrons and ions. Electrostatic interactions between electrons are negligible throughout most of the envelope for the temperatures of interest (see Chabrier & Potekhin 1998), and the electrons are an ideal degenerate Fermi gas for $\psi = \mu_{\rm e}/k_{\rm B}T \gg 1$. Here $\mu_{\rm e}$ is the electron chemical potential, not including the rest mass. For $\psi \gg 1$, $\mu_{\rm e} \approx (\varepsilon_{\rm F} - m_{\rm e}c^2)$, where $\varepsilon_{\rm F} = (m_{\rm e}^2c^4 + p_{\rm F}^2c^2)^{1/2}$ is the electronic Fermi energy and $p_{\rm F} = (3\pi^2 n_{\rm e})^{1/3}\hbar$ is the Fermi momentum. We write the electron density $n_{\rm e} \equiv Y_{\rm e}\rho/m_{\rm u}$ where $m_{\rm u}$ is the mean nucleon mass and delimit on Figure 1 where the electrons are degenerate with the condition $\psi = 10$ (*dashed line*). The electrons are relativistic where $p_{\rm F}/m_{\rm e}c \approx [Y_{\rm e}\rho/(10^6\ {\rm g\ cm^{-3}})]^{1/3} > 1$.

Where the envelope is composed of rp-process ashes, the total number of species (each of density n_j) is likely quite large. Electrostatic correlations between ions are parameterized by

$$\Gamma_j = \frac{Z_j^2 e^2}{a_j k_{\rm B} T} \approx Z_j^{5/3} \left(\frac{Y_{\rm e}\rho}{10^8\ {\rm g\ cm^{-3}}}\right)^{1/3} \left(\frac{10^8\ {\rm K}}{T}\right), \quad (3)$$

$a_j = (3Z_j/4\pi n_{\rm e})^{1/3}$ being the ion sphere radius for species j. For $\Gamma > \Gamma_{\rm M}$, the plasma is a solid; $\Gamma_{\rm M}$ is computed by equating the free energies of the liquid and solid phases (Fig. 1, *solid line*). We compute the ionic free energy for the liquid phase, $1 \le \Gamma < \Gamma_{\rm M}$, from the fit of Chabrier & Potekhin (1998) and for the solid phase from the fit of Farouki & Hamaguchi (1993). In a recent calculation, Potekhin & Chabrier (2000) determined that $\Gamma_{\rm M} = 175.0 \pm 0.4$, with a further relative uncertainty of ~ 10 % arising from electron screening. The calculations in this paper are insensitive, fortunately, to the precise value of $\Gamma_{\rm M}$.

The ions are classical for

$$\theta = \frac{T}{T_{\rm p,ion}} = \frac{k_{\rm B}T}{\hbar}\left(\frac{\langle A\rangle^2 m_{\rm u}^2}{4\pi\rho\langle Z\rangle^2 e^2}\right)^{1/2} \approx \left(\frac{T}{4.0\times10^7\ {\rm K}}\right)\left(\frac{10^8\ {\rm g\ cm^{-3}}}{\rho}\right)^{1/2}\left(\frac{\langle A\rangle}{2\langle Z\rangle}\right) \gg 1, \quad (4)$$

where θ is the temperature in units of the ion plasma temperature. The ratio of melting to plasma temperatures is

$$\frac{T_{\rm M}}{T_{\rm p,ion}} = 3.4\left(\frac{175}{\Gamma_{\rm M}}\right)\left(\frac{\langle Z\rangle}{30}\right)^{5/3}\left(\frac{2\langle A\rangle}{\langle Z\rangle}\right)^{2/3}\left(\frac{10^8\ {\rm g\ cm^{-3}}}{\rho}\right)^{1/6} \quad (5)$$

and so $T \gtrsim T_{\rm p,ion}$ wherever the ions are composed of high-Z species and are in a liquid phase. When $\theta < 1$ (*dotted lines*, Fig. 1), quantum lattice effects become important. As evident from Fig. 1, in a H layer the ions are typically weakly coupled throughout, although one should be careful about quantum plasma effects (for a discussion,

see Potekhin et al. 1997). In contrast, the ions in a ^{104}Ru layer are strongly coupled wherever the electrons are degenerate. Quantization of phonon modes is not important, however, except in the very degenerate layers where the thermal gradient is nearly isothermal.

3.2. *Sedimentation*

The calculation in this paper presumes that the envelope is segregated into layers. An order-of-magnitude calculation illustrates the timescale for the envelope to become stratified. In a frame co-moving with the mean ion center-of-mass (CM; here at rest), the continuity equation for species i is

$$\frac{\mathrm{d}n_i}{\mathrm{d}t} = \boldsymbol{\nabla}\cdot\left(\mathcal{D}\boldsymbol{\nabla}n_i - n_i\boldsymbol{w}_i\right), \tag{6}$$

where $\mathcal{D}$ is the interspecies diffusion coefficient and $\boldsymbol{w}_i$ and n_i are respectively the drift velocity, relative to the mean ion CM, and the number density of species i. This equation neglects terms arising from thermal diffusion, which are generally small in dense ionic plasmas (Stevenson & Salpeter 1977; Paquette et al. 1986).

The diffusion coefficient, $\mathcal{D}$, and the drift velocity, $\boldsymbol{w}$, are both local quantities, i.e., they do not depend on $\boldsymbol{\nabla}\rho$ or $\boldsymbol{\nabla}T$. For a trace component (species "2") in a background (species "1") these quantities are effectively fixed, and are therefore related through Einstein's relation (see, e.g., Landau & Lifshitz 1987), $\boldsymbol{w}_2 = \left[\mathcal{D}/(k_{\rm B}T)\right]\boldsymbol{F}_2$ where $\boldsymbol{F}_2$ is the force on the trace ion and the combination $\mathcal{D}/(k_{\rm B}T)$ is the mobility. This relation holds where the temperature scale height $-[\mathrm{d}(\ln T)/\mathrm{d}r]^{-1} \gg H_p = p/\rho g$, the pressure scale height. Since $-H_p[\mathrm{d}(\ln T)/\mathrm{d}r] = \mathrm{d}(\ln T)/\mathrm{d}(\ln p) < (\partial \ln T/\partial \ln p)_s < 1$, this requirement is trivially satisfied. The force $\boldsymbol{F}_2$ is the sum of gravity and the electric field needed to keep the ions from settling relative to the electrons (see, e.g., Spitzer 1962; Hameury et al. 1983),

$$\begin{aligned}\boldsymbol{F}_2 &= A_2 m_{\rm u}\boldsymbol{g} - Z_2 e\boldsymbol{E} \\ &= \begin{cases} \left(A_2 - \frac{Z_2 A_1}{Z_1+1}\right) m_{\rm u}\boldsymbol{g}, & \text{non-degenerate} \\ \left(A_2 - \frac{Z_2 A_1}{Z_1}\right) m_{\rm u}\boldsymbol{g}, & \text{degenerate.} \end{cases}\end{aligned} \tag{7}$$

The electric field is $e\boldsymbol{E} = m_{\rm u}\boldsymbol{g}\left[A_1/(Z_1+1)\right]$ where the electrons are nondegenerate and $e\boldsymbol{E} = m_{\rm u}\boldsymbol{g}(A_1/Z_1)$ where they are degenerate and contribute most of the gas pressure.

From continuity (eq. [6]) the timescale for the trace ions to move a distance s is $\tau_{\rm dr} = \min(s^2\mathcal{D}^{-1}, s\|\boldsymbol{w}_2\|^{-1})$, where the first term is the diffusion timescale and the second is the drift timescale. These timescales are equal for $s = H_2 = k_{\rm B}T/\|\boldsymbol{F}_2\|$, which is just the scale height for the trace ions. For mass/charge ratios much greater than unity and where the electrons are degenerate, $H_2 \ll H_p$; therefore over macroscopic scales $s \sim H_p$, the relevant timescale is the drift timescale $\tau_{\rm dr} = s\|\boldsymbol{w}_2\|^{-1} = sF_2(k_{\rm B}T/\mathcal{D})$. We can evaluate $\tau_{\rm dr}$ once the mobility is determined. For the situation in question ($y \sim 10^8$ g cm^{-2}, $T \sim 10^8$ K), the background matter exists in a liquid phase ($1 < \Gamma_1 < \Gamma_{1,\rm M}$) (see Figure 1). We follow the calculation of Bildsten & Hall (2001) and estimate $\mathcal{D}$ from the Stokes-Einstein relation between the mobility and the drag coefficient (for a liquid sphere), $\mathcal{D}/k_{\rm B}T = 1/(4\pi a_2\eta)$. In this expression, a_2 is the radius of a charge-neutral (containing Z_2 electrons) sphere around the trace particle and η is the viscosity of the material. Fits to numerical simulations of one-component plasmas (OCP) in the liquid regime find that the viscosity is $\eta \approx (0.1\ \mathrm{g\ cm^{-1}\ s^{-1}})(\rho/\mathrm{g\ cm^{-3}})(\omega_{\rm p,1}/\mathrm{s^{-1}})(a_1^2/\mathrm{cm^2})(\Gamma_1/10)^{0.3}$, where a_1 is the ionic spacing of the background fluid and $\omega_{\rm p,1} = \left[4\pi\rho(Z_1 e/A_1 m_{\rm u})^2\right]^{1/2}$ is the plasma frequency (Donko & Nyiri 2000; Bildsten & Hall 2001).

Using the non-relativistic degenerate electron equation of state to relate p and ρ and evaulating $\boldsymbol{F}_2$ from equation (7), we find from the Stokes-Einstein relation the mobility,

$$\frac{\mathcal{D}}{k_{\rm B}T} \approx 1.2\times10^7\ \mathrm{s\ g^{-1}}\ \frac{A_1^{0.1}T_7^{0.3}}{Z_1^{1.3}Z_2^{0.3}\rho_5^{0.6}}. \tag{8}$$

For brevity we scale the surface gravity, temperature, and density to $g = g_{14}10^{14}$ cm s^{-2}, $T = T_7 10^7$ K, and $\rho = \rho_5 10^5$ g cm^{-3}. The value $\mathcal{D}$ computed from equation (8) is comparable (within a factor of a few) to that calculated by Tanaka & Ichimaru (1987) for a strongly coupled OCP under the conditions of interest. It is somewhat larger than the value estimated with the formalism of Chapman & Cowling (1952) or Burgers (1969), both of which are valid for weakly coupled plasmas, $\Gamma \ll 1$ (also see Fontaine & Michaud 1979; Paquette et al. 1986).

Upon substituting equation (8) into the expression for $\boldsymbol{w}_2$ and using H_p as a fiducial lengthscale, one arrives at the stratification timescale,

$$\tau_{\rm dr} \approx 10^5\ \mathrm{s}\left[\frac{Z_1^{3.9}Z_2^{0.3}\rho_5^{1.3}}{A_1^{1.8}g_{14}^2T_7^{0.3}(A_2Z_1 - A_1Z_2)}\right]. \tag{9}$$

For ^{104}Ru in ^{4}He at $\rho_5 = 1$, $T_7 = 10$, and $g_{14} = 1$ (appropriate for Aql X-1; § 5), equation (9) implies that the ^{104}Ru ions settle in a time of roughly 2 hr. For ^{56}Fe in ^{4}He, the timescale is roughly 7 hr. For the less dense regions of the envelope, the diffusive time scale is of order seconds to minutes, so in the absence of any circulation the envelope quickly stratifies after the end of the accretion outburst. Our calculations throughout the remainder of the paper assume a fully stratified envelope. We note that in diffusive equilibrium, the boundary between the layers has a thickness $\sim H_2 \ll H_p$, which justifies our approximating the interface as a planar surface.

3.3. *Thermal Transport*

For the temperatures and densities in the quiescent neutron star envelope, the relevant opacities are Thomson scattering and free-free absorption. Because the outermost layers are composed of H and ^{4}He, the ions are fully ionized throughout. At typical envelope temperatures, the dominant opacity is from free-free absorption,

$$\kappa_{\rm ff} \propto n_{\rm e}T^{-7/2}\sum_j Z_j^2 Y_j g_{{\rm ff},j} \tag{10}$$

where the Gaunt factor for species j, $g_{{\rm ff},j}$, contains corrections for electronic Coulomb wavefunctions, degeneracy, and relativistic effects. There are no fits of $g_{\rm ff}$ that cover the entire (ρ, T) range appropriate for this problem. The relation between $T_{\rm b}$ and $T_{\rm eff}$ is most sensitive to κ where the electrons are semi-degenerate, however, so we use the

fit from Schatz et al. (1999) that is tuned to be accurate for $\psi \lesssim 10$ and moderately strong Coulomb corrections, parameterized by $-4 < \ln\gamma^2 = Z^2e^4m_e/(2\hbar^2k_BT) < 2$. This fit is reasonably accurate (fractional errors ~ 10 %) when compared against the calculations of Itoh et al. (1985, 1991). We calculate the Thomson scattering opacity by using a fit (Buchler & Yueh 1976) that reproduces the non-degenerate limit (Sampson 1959) and includes corrections for the relativistic and degenerate electronic EOS.

As ψ increases, the degenerate electrons become more efficient than photons at transporting heat. The electron thermal conductivity is given in the relaxation-time approximation by the Wiedemann-Franz law,

$$K = \frac{\pi^2}{3}\frac{n_e k_B^2 T}{m_e^\star}\tau, \tag{11}$$

where $m_e^\star = \varepsilon_F/c^2$ is the effective electron mass, and τ is the electron thermal distribution relaxation time. In this approximation, the relaxation time is the reciprocal sum over electron-electron and electron-ion scattering relaxation times, $\tau^{-1} = \tau_{e,e}^{-1} + \tau_{e,ion}^{-1}$. In the heavy element layer, the large values of Γ (see Fig. 1) may inhibit stratification, and therefore we must consider a multi-species plasma. Where $\theta \gtrsim 1$, a reasonable approximation (motivated by the additivity rule in multi-ionic EOS; Potekhin et al. 1999) is to sum over inverse relaxation times for each species, $\tau_{e,ion}^{-1} = \sum_j \tau_{e,j}^{-1}$, where $\tau_{e,j}$ are the separate inverse relaxation times for electron-electron and electron-ion (from species j) scattering, respectively. We calculate the electron-electron scattering relaxation time from the formalism of Urpin & Yakovlev (1980), as fit by Potekhin et al. (1997). The inverse electron-ion scattering relaxation time is

$$\tau_{e,ion}^{-1} = \frac{4\pi e^4}{p_F^2 v_F}\frac{\rho}{m_u}\sum_j Z_j^2 Y_j \Lambda_{e,j}. \tag{12}$$

Here $v_F = p_F/m_e^\star$ is the electron velocity evaluated at the Fermi surface, and $\Lambda_{e,j}$ is the dimensionless Coulomb logarithmic term that originates in the integration of the scattering rate over electron phase space. To evaluate $\Lambda_{e,j}$, we use the fitting formula of Potekhin et al. (1999), which is straightforward to implement for arbitrary (Z, A).

Where $\theta \lesssim 1$, phonon modes begin to "freeze out," and the additivity rule (eq. [12]) becomes suspect. In practice this is not typically a concern, because scattering from charge *fluctuations* (impurity scattering) becomes more important than electron-phonon scattering. If the impurities are randomly distributed, then the "structure factor" in the integration of the scattering integral can be set to unity (Potekhin, private communication; also see Itoh & Kohyama 1993), and $\Lambda_{e,imp}$ resembles that of the liquid ($\Gamma \ll \Gamma_M$) phase with a relaxation time depending on the rms charge difference,

$$\tau_{imp}^{-1} = \frac{4\pi e^4}{p_F^2 v_F}\frac{\rho}{m_u}\sum_j \left(Z_j - \langle Z\rangle\right)^2 Y_j \Lambda_{e,imp}. \tag{13}$$

Thus the scattering differs from that in a liquid by a factor

$$\frac{\langle Z^2\rangle}{\langle Z\rangle^2} - 1 \equiv \frac{Q}{\langle Z\rangle^2} \tag{14}$$

With the structure factor in eq. (8) of Potekhin et al. (1999) set to unity, we find that the resulting $\Lambda_{e,imp}$ is comparable to the fit given by Itoh & Kohyama (1993).

How large might Q be? The output from a one-zone X-ray burst nucleosynthesis calculation (Schatz et al. 2001) has $Q/\langle Z\rangle^2 = 233/37^2 = 0.17$. The computation of $\Lambda_{e,j}$ assumes that the separate species are arranged in a lattice; it is difficult to imagine how this could come about in the case of an accreted neutron star crust. For the conditions of interest in this paper ($\rho \lesssim 10^{10}$ g cm^{-3}, $T \lesssim 10^8$ K, and an rp-process ash composition), $\tau_{imp}^{-1} \lesssim \sum_j \tau_{e,j}^{-1}$. Impurity scattering is therefore not dominant, unlike the case in the deep crust (Brown 2000; Gnedin et al. 2001); it is also not negligible, however, so the question arises as to how the two scattering processes should add. Such a calculation, while clearly important, is beyond the scope of this paper. We instead take a pragmatic approach and use two different prescriptions:

$$\tau_{e,ion}^{-1} = \frac{4\pi e^4}{p_F^2 v_F}\frac{\rho}{m_u}\max\left(\sum_j Z_j^2 Y_j \Lambda_{e,j}, \frac{Q}{\langle A\rangle}\Lambda_{e,imp}\right) \tag{15}$$

and

$$\tau_{e,ion}^{-1} = \frac{4\pi e^4}{p_F^2 v_F}\frac{\rho}{\langle A\rangle m_u}\left(\langle Z\rangle^2\bar{\Lambda}_{e,ion} + Q\Lambda_{e,imp}\right). \tag{16}$$

Here $\bar{\Lambda}_{e,ion}$ is the Coulomb logarithm for a single ion of charge number $\langle Z\rangle$ and mass number $\langle A\rangle$. Both approaches give comparable results in the Debye screening limit ($\theta \to 0$) and in the limit ($\theta \gg 1$) where impurity scattering dominates. In the regime where both impurity and phonon scattering are comparable, the second prescription (eq. [16]) gives a larger $\tau_{e,ion}^{-1}$ and hence a smaller K. For purposes of comparison (§ 4) we compare the conductivity of a pure state, e.g., ^{104}Ru with that obtained using equation (16); this gives the largest variation in K.

3.4. *Sensitivity*

The choice of input physics can dramatically affect the relation $T_{eff} = T_{eff}(T_b)$. The greatest uncertainty lies with the calculation of conductive opacities around the melting point, $\Gamma \approx \Gamma_M$, and in the crystalline phase. This is partly due to our ignorance of the exact composition of the envelope. We consider in §§ 4 and 5 different possibilities for the composition of the heavy elements: ^{56}Fe, ^{104}Ru, and the rp-process ashes. In this section we consider how a different prescription for the electron-ion conductivity (Flowers & Itoh 1981; Itoh et al. 1983; Itoh & Kohyama 1993) than our adopted formulae (Potekhin et al. 1999) would change our results. By looking at the sensitivities of our results to the choice of conductivity, we can understand how our results vary in response to the general uncertainties in input physics.

Figure 2 highlights this problem. Away from the melting point in the liquid regime, the fitting formulae given by Potekhin et al. (1999), $\kappa_{Pot.}$, and Itoh & Kohyama (1993), κ_{Itoh}, are in good agreement, $|1 - \kappa_{Pot.}/\kappa_{Itoh}| \approx$ 5 %–60 %. The agreement begins to fall apart near the melting point and the conductivities in the crystalline regime differ by a factor of 2–3 (for a discussion, see Potekhin et al. 1999). Because our conductivity is uncertain, in any case, for a multi-species plasma (§ 3.3), we consider how variations in the thermal conductivity affect the relation between T_b and T_{eff}.

For a neutron star envelope of fixed composition with a given $T_{\rm eff}$, the temperature profile $T(y)$ can roughly be divided into three regions: the radiative zone, $\kappa_{\rm c} \gg \kappa_{\rm r}$; the sensitivity strip, $\kappa_{\rm c} \approx \kappa_{\rm r}$; and the isothermal zone $\kappa_{\rm c} \gg \kappa_{\rm r}$. The sensitivity strip is so named because changes to the conductive opacity in this region strongly affect the temperature profile of the envelope (Gudmundsson et al. 1983; Potekhin et al. 1997; Ventura & Potekhin 2002). A change in the conductive opacity in the sensitivity strip changes the region where the sensitivity strip lies. Since this region controls the transition from a power law radiative solution to a isothermal zone solution, it is critical that the conductive opacity be well-understood here.

The location of the sensitivity strip $y_{\rm ss}$ is roughly where $\kappa_{\rm c} \approx \kappa_{\rm r}$. Setting $\kappa_{\rm c} = C\kappa_{\rm r}$ (where C is an arbitrary constant that contains our uncertainty regarding the composition and scattering integrals in $\kappa_{\rm c}$ and $\kappa_{\rm r}$), using an ideal gas equation of state, and setting factors of order unity to unity, we find that

$$y_{\rm ss} \approx 2.2 \times 10^3 \ {\rm g \ cm^{-2}} \left[C^{-1/3} \frac{A^2 Z}{(Z+1) g_{14}} T_7^{17/6} \right]. \quad (17)$$

To relate $y_{\rm ss}$ to $T_{\rm eff}$, we insert the solution to the flux equation (eq. [1]) in the radiative zone. Since the dominant opacity is from free-free absorption, we can take as our opacity $\kappa \propto \rho T^{-7/2}$. Inserting this into equation (1) and again using an ideal gas equation of state, we find that $y^2 \propto T^{17/2}$. Solving for T and inserting all the appropriate numerical factors, we have

$$T_7 = 0.16 y^{4/17} \left[\frac{Z^3 g_{14} T_{\rm E,6}^4}{A(Z+1)} \right]^{2/17}. \quad (18)$$

Inserting the expression for $y_{\rm ss}$, equation (17), into equation (18), one finds that the temperature in the sensitivity strip scales as $T_{\rm ss} \propto C^{-4/17}$. To estimate how $T_{\rm eff}$ scales with the microphysical input, we note that if $T_{\rm ss} \approx T_{\rm b}$ then $T_{\rm eff} \propto C^{1/2}$. Therefore, this calculation is moderately sensitive to fractional uncertainties of order 10 % in the input physics. Since the sensitivity strip is in the regime where the envelope matter remains a liquid (Ventura & Potekhin 2002), our sensitivity to the microphysics of the crystalline matter is relatively small, especially for the surface temperatures ($T_{\rm eff} \sim 10^6$ K) of interest.

4. THE VARIATION OF EFFECTIVE TEMPERATURE

Having laid out our microphysical tools, we are now ready to explore how the changing envelope stratification varies the relation between the deep crust temperature $T_{\rm b}$ and the effective temperature $T_{\rm eff}$. To do this, we adopt a two-layer model with a variable column depth $y_{\rm i}$ of the top layer. The outer layer is composed of H or ^{4}He, and the inner layer either pure ^{56}Fe, ^{104}Ru, or ashes from rp-process burning. We integrate equation (1) numerically using an Adams predictor-corrector method (Hindmarsh 1983). As a boundary condition for equation (1), we apply the Eddington approximation[2] at the photosphere, $\kappa(\rho, T_{\rm eff}) y_{\rm ph} = 2/3$. For a given $T_{\rm eff}$, we then integrate equation (1) inwards to $y_{\rm b} = 10^{14}$ g cm^{-2}. At this column, the thermal gradient becomes nearly isothermal, and $T_{\rm b} = T(y = y_{\rm b})$ is approximately the interior temperature. The inverse relation $T_{\rm eff}(T_{\rm b})$ is then found by iteration. As a check, we compared our calculations to those of Potekhin et al. (1997) for a ^{56}Fe envelope and a "fully accreted" envelope (H/He/C/Fe layers). For a given $T_{\rm b}$, the fractional difference between our value of $T_{\rm eff}$ and that computed from the fitting formula of Potekhin et al. (1997) is of order 5 %, with the largest deviation occurring when the H/^{56}Fe interface is in the sensitivity strip.

To illustrate how the opacity changes with the variation in the *location* of the interface, we show in Figure 3 a two-layer neutron star envelope (H superincumbent on ^{104}Ru) with $y_{\rm i} = 10^{4.4}$ g cm^{-2} (panels a, c) or $y_{\rm i} = 10^{8.13}$ g cm^{-2} (panels b, d). In both cases $T_{\rm b} = 7.5 \times 10^7$ K. The two top panels (a, b) depict the temperature, while the bottom panels (c, d) display the total opacity (*solid line*), radiative opacity (*dotted line*), and conductive opacity (*dashed line*). When the interface is at a low column, both the radiative and conductive opacities play a role. At higher column, the conductive opacity dominates at the location of the interface. In both cases there is a substantial increase in the opacity of a ^{104}Ru layer from a H layer, reflecting the increase in the ion charge for bremsstrahlung and electron-ion scattering.

At low densities, the opacity is dominated by radiative processes (mostly free-free). For a free-free dominated envelope, $T(y) \propto y^{4/17}$ (eq. [18]); as a result, along the trajectory $\{y, T(y)\}$, the free-free opacity is $\kappa_{\rm ff} \propto y^{-1/17}$ (Fig. 3, *dotted lines*) and is nearly constant. As the composition changes from H to ^{104}Ru, the opacity jumps by a factor $\approx 44^2/104$. Where the electrons are degenerate and the heat transport set by electron conduction, ${\rm d}T/{\rm d}y \rightarrow 0$, and the Gaunt factor scales as $n_{\rm e}^{-2/3}$, so $\kappa_{\rm ff} \propto y^{1/4}$. In the limit where the electrons are degenerate and relativistic, the electron conductive opacity scales as $\kappa_{\rm c} \propto [T(y)]^2/y$, and $T(y)$ is nearly constant. The jump at the interface is $\Delta\kappa_{\rm c} < Z^2/A = 44^2/104$ because the stronger ion-ion correlations (parameterized by Γ) decrease the scattering rate $\tau_{{\rm e},j}^{-1}$ and offset the increase from the larger ionic charge.

Figure 4 shows the emergent flux ($T_{\rm eff}^4$) for a two-layer neutron star envelope as a function of $y_{\rm i}$. The top layer is either pure H (*thin lines*) or ^{4}He (*thick lines*), and the bottom layer is composed of either ^{56}Fe (*solid lines*), ^{104}Ru (*dotted lines*), or an rp-process mixture with the mean-ion approximation (eq. [16]; *dashed lines*). For each composition, we used 4 bottom temperatures: $T_{\rm b} = 3.75 \times 10^7$ K, 7.5×10^7 K, 1.5×10^8 K, and 3.0×10^8 K. The difference in $T_{\rm eff}^4$ between an outer H layer and an outer ^{4}He layer is typically smaller than the difference between the different ash compositions and locations of the interface. Were we to calculate $\tau_{\rm e,ion}$ using equation (15) rather than equation (16), the resulting curves would have lain between those of an ^{104}Ru layer (*dotted lines*) and the rp-ashes with the mean-ion approximation (*dashed lines*). The emergent flux is insensitive to the location of the interface for $y \lesssim 10^5$ g cm^{-2}; as the interface moves deeper the lower opacity of H layer reduces $|{\rm d}T/{\rm d}y|$ so that $T_{\rm eff}$ increases for a fixed $T_{\rm b}$. Note also that the profile for the multi-

[2] The value of $T_{\rm b}$ for a given $T_{\rm eff}$ is insensitive to the precise location of the photosphere, so this approximation is sufficient for our purposes.

species ash has a lower $T_{\rm eff}$ (higher opacity) than that of a pure ^{104}Ru layer despite having a smaller $\langle Z \rangle$. Because the Γ_j for each species in a multi-component mixture is reduced relative to that for a pure species, $\Lambda_{{\rm e},j}$ is larger at high densities, where $\theta \lesssim 1$.

By how much can the depth of the outermost layer vary? The maximum depth of the H layer is set by the reaction p(e^-,ν)n. This reaction occurs for $\varepsilon_{\rm F} > m_{\rm n} - m_{\rm p} + m_{\rm e} = 1.29$ MeV, or $\rho \approx 1.3 \times 10^7$ g cm^{-3}. With our assumed surface gravity, the corresponding column is $y = 1.6 \times 10^{10}$ g cm^{-2}. For a pure ^{4}He layer, the maximum depth would be where the strongly screened 3α reaction (Fushiki & Lamb 1987) ignites: $\rho > 10^8$ g cm^{-3} for temperatures $< 10^8$ K. Accretion to this depth requires a very slow accretion rate over a long time. For the column accretion rate needed to power the quiescent thermal emission, $\dot{m} \approx 1$ g cm^{-2} s^{-1}, the time needed to accrete H to the electron capture depth is 500 yr. This could possibly occur for long-recurrence time transients such as KS 1731−260 (Rutledge et al. 2001c; Wijnands et al. 2001). For short recurrence-time transients, such as Aql X-1, the H layer cannot be appreciably thicker than where ^{4}He unstably ignites, $y_{\rm ign} \approx 10^8$ g cm^{-2} (see Bildsten 1998, and references therein). How *thin* the light-element layer might be is more difficult to determine. As noted in §2, the column of H deposited after the last burst for spherically symmetric accretion is $\lesssim y_{\rm ign}$. If the accretion were to occur onto only a small fraction of the surface and then later spread over the surface, than the residual column could be much less than $y_{\rm ign}$.

5. AQL X-1, CEN X-4, AND SAX J1808.4−3658

Having explored the variation induced in $T_{\rm eff}$ by varying $y_{\rm i}$ and the composition of the envelope, we now describe the thermal structure of Aql X-1, Cen X-4, and SAX J1808.4−3658. Aql X-1 and Cen X-4, despite having similar binary orbital periods (19 hr and 15.1 hr, respectively), have very different outburst morphologies: Aql X-1 goes into an ≈ 30 d outburst on a roughly yearly basis, while Cen X-4 has had just two recorded outbursts (only one of which contributed significantly to the total observed fluence) in the past 33 yr. SAX J1808.4−3658 is distinguished from both Cen X-4 and Aql X-1 by virtue of having pulsations (Wijnands & van der Klis 1998) in the persistent emission; its orbital period is also much shorter (2.01 hr; Chakrabarty & Morgan 1998), and it quite possibly accretes from a substellar mass companion (this also explains its low time-averaged accretion rate, $\langle \dot{M} \rangle \sim 10^{-11}\ M_\odot$ yr^{-1}; Bildsten & Chakrabarty 2001). Figure 5 displays a summary of calculations for these three objects: from top to bottom, Aql X-1 ($T_{\rm eff} = 2.1 \times 10^6$ K), Cen X-4 ($T_{\rm eff} = 8.8 \times 10^5$ K), and SAX J1808.4−3658 ($T_{\rm eff} = 6.8 \times 10^5$ K). We fix the composition of the outer layer to be ^{4}He (*solid line*) with a column $y_{\rm i} = 10^8$ g cm^{-2}, and vary the composition of the inner layer between ^{56}Fe (*dotted line*), ^{104}Ru (*dashed line*), and rp-process ashes (*dot-dashed line*). We now explain each calculation in more detail.

Chandra observations of Aql X-1 (Rutledge et al. 2001a) find that $k_{\rm B}T_{\rm eff,\infty} = 135^{+18}_{-12}$ eV. For a fiducial neutron star of mass $M = 1.4\ M_\odot$ and $R = 10$ km, the proper effective temperature is $T_{\rm eff} = T_{\rm eff,\infty}(1+z) = 2.1 \times 10^6$ K. At this temperature and $y_{\rm i}$, the fractional difference in $T_{\rm b}$ between an outer layer composed of H and one composed of ^{4}He is $T_{\rm b}({\rm H})/T_{\rm b}(^4{\rm He}) - 1 < 0.02$. Using Figure 4, the variation in the emergent flux induced by a changing $y_{\rm i}$ is, at this $T_{\rm b}$, roughly a factor of 2; changing the composition of the ash from ^{56}Fe to rp-process ashes increases $T_{\rm eff}^4$ by a factor ≈ 1.6.

This calculation is consistent with widely spaced observations of Aql X-1, which find variability by a factor of 1.9 over a timescale of years (i.e., over several outburst/recurrence timescales). We cannot explain changes on timescales less than this, however. As mentioned in § 1, Rutledge et al. (2002a) observed Aql X-1 with *Chandra* on four successive occasions following the November 2000 outburst. The intensity was observed to decrease by a factor of ≈ 0.5 over 3 months and then increase by a factor of ≈ 1.4 over 1 month. In addition, short timescale ($< 10^4$ s) variability was evident in the last observation. Our present calculation does not address the short timescale variability. The fact that the intensity first decreased and then increased also cannot be accomodated in the scenario we outline in this paper. Moreover, the timescale for sedimentation (eq. [9]) is far too brief.

For Cen X-4, *Chandra* observations find that $k_{\rm B}T_{\rm eff} = (76 \pm 7)$ eV (Rutledge et al. 2001b). The last known accretion outburst occurred in 1979. Assuming no outbursts have occurred since then, the crust has had several thermal times to relax. As with Aql X-1, we again set the outer layer to be pure ^{4}He (Fig. 5; *solid line*). The reason we choose the outer layer to be ^{4}He reflects our prejudice that H is consumed as the accretion rate decreases at the end of the outburst. Changing the outer layer to H increases $T_{\rm b}$ by a factor $T_{\rm b}({\rm H})/T_{\rm b}(^4{\rm He}) - 1 < 0.08$. For transients with recurrence times of decades or longer, such as Cen X-4 and KS 1731−260, it is possible that residual accretion could substantially *increase* the depth of the H/^{4}He layer. Wijnands et al. (2001) and Rutledge et al. (2001c) found the luminosity of KS 1731−260 to be $\approx 3 \times 10^{33}$ ergs s^{-1}; this constrains the quiescent accretion rate to $\dot{M}_q \lesssim 2 \times 10^{-13}\ M_\odot$ yr^{-1}. Accretion at this limiting rate increases $y_{\rm i}$ by 10^8 g cm^{-2} every 30 years. By itself, this can change the brightness by a factor of 1.2 on this timescale. This effect may be dwarfed by the thermal relaxation of the crust, however, which also occurs over a timescale of decades (Rutledge et al. 2001c). A simulation of the time-dependent thermal luminosity for such sources is beyond the scope of this introductory paper; for now we just note this interesting possibility.

Finally, we turn our attention to SAX J1808.4−3658. This source is rather dim in quiescence (Stella et al. 2000; Dotani et al. 2000; Wijnands et al. 2002). We estimate the surface effective temperature from the flux reported by Wijnands et al. (2002); note that this is not a bolometric flux, and may also include a contribution from a power-law. For the estimated temperature, the overall stratification is similar to that of Cen X-4, with $T_{\rm b} \approx 2.8 \times 10^7$ K. The variation in $T_{\rm eff}$ is approximately a factor of 4 at $T_{\rm eff} < 10^6$ K. Given its short recurrence time and cold $T_{\rm eff}$, SAX J1808.4−3658 may be the best source from which to observe the effect described in this paper. If the previous few years are typical, then either *Chandra* or *XMM* can

likely observe different quiescent epochs.

6. SUMMARY AND DISCUSSION

In summary, we find that (1) the timescale for the neutron star envelope to segregate into layers is much less than the outburst recurrence time, making the surface effective temperature sensitive to the mass of H/^{4}He remaining on the surface at the end of an outburst; (2) variations in the composition of the heat-blanketing envelope can lead to variability, by a factor of 2 to 3, in the *thermal* quiescent flux from neutron star SXTs; (3) the crust temperatures of Aql X-1, Cen X-4, and SAX J1808.4−3658, for the quoted effective temperatures, are respectively 3.3×10^8 K, 4.9×10^7 K, and 2.8×10^7 K with a fractional uncertainty, from $y_{\rm i}$ and the ash composition, of roughly 20 %.

The measured $T_{\rm eff}$ and inferred $T_{\rm b}$ of Aql X-1 have interesting implications for the interior temperature of the neutron star. As described in Brown (2000), when the temperature in the crust is sufficiently hot, there is an inversion of dT/dr: heat flows *inward* from the crust to the core, where it is balanced by the neutrino luminosity L_ν. A calculation similar to that described in Brown & Ushomirsky (2000), with the "moderate superfluid" case discussed in Brown (2000) finds that the ratio of quiescent photon luminosity to neutrino luminosity is $L_{\rm q}/L_\nu = 3.6$. Our choice of superfluid transition temperatures in these calculations are similar to those employed by Yakovlev et al. (2001) in fitting to observations of cooling neutron stars. This suggests that for sources with higher $\langle L \rangle$ than Aql X-1, the simple distance-independent relation between the quiescent flux and the time-averaged outburst flux (Brown et al. 1998) does not exactly hold. For sources with lower $\langle L \rangle$, neutrino cooling is not important, unless an enhanced (beyond modified Urca; see Colpi et al. 2001) neutrino emissivity operates. A direction for future work would be to incorporate recent fits (Kaminker et al. 2001) of cooling neutron star observations.

We reiterate that the best place to observe the effect of a changing light-element layer mass is a source such as SAX J1808.4−3658, which has both a low $T_{\rm eff}$ (Wijnands et al. 2002) and a short recurrence timescale (2 outbursts in the past 6 years). At lower $T_{\rm b}$, the effective temperature can vary by as much as a factor of 4, while the frequent outbursts allow comparison between different envelope layerings for a fixed core temperature.

We thank A. Potekhin for educating us on the thermal conductivity and for carefully reading the manuscript and F. Timmes for providing us with tables and interpolation routines for the electronic equation of state. This work is partially supported by the Department of Energy under grant B341495 to the Center for Astrophysical Thermonuclear Flashes at the University of Chicago, by the National Science Foundation under Grants PHY 99-07949 and AST 01-96422, and by NASA through grant NAG 5-8658. E. F. B. acknowledges support from an Enrico Fermi fellowship. L. B. is a Cottrell Scholar of the Research Corporation.

REFERENCES

Bildsten, L. 1998, in The Many Faces of Neutron Stars, ed. A. Alpar, R. Buccheri, & J. van Paradijs, Vol. 515, NATO ASI ser. C (Dordrecht: Kluwer), 419
Bildsten, L. 2000, in Cosmic Explosions, ed. S. S. Holt & W. W. Zhang, 359
Bildsten, L. & Chakrabarty, D. 2001, ApJ, 557, 292
Bildsten, L. & Hall, D. M. 2001, ApJ, 549, 219
Bildsten, L., Salpeter, E. E., & Wasserman, I. 1992, ApJ, 384, 143
Bisnovatyi-Kogan, G. S. & Chechetkin, V. M. 1979, Soviet Phys.-Uspekhi, 127, 263
Brown, E. F. 2000, ApJ, 531, 988
Brown, E. F., Bildsten, L., & Rutledge, R. E. 1998, ApJ, 504, L95
Brown, E. F. & Ushomirsky, G. 2000, ApJ, 536, 915
Buchler, J. R. & Yueh, W. R. 1976, ApJ, 210, 440
Burgers, J. M. 1969, Flow Equations for Composite Gases (New York: Academic Press, Inc.)
Campana, S., Colpi, M., Mereghetti, S., Stella, L., & Tavani, M. 1998, A&A Rev., 8, 279
Campana, S., Mereghetti, S., Stella, L., & Colpi, M. 1997, A&A, 324, 941
Chabrier, G. & Potekhin, A. Y. 1998, Phys. Rev. E, 58, 4941
Chakrabarty, D. & Morgan, E. H. 1998, Nature, 394, 346
Chapman, S. & Cowling, T. G. 1952, The Mathematical Theory of Non-Uniform Gases (Cambridge: Cambridge University Press)
Colpi, M., Geppert, U., Page, D., & Possenti, A. 2001, ApJ, 548, L175
Donko, Z. & Nyiri, B. 2000, Phys. Plasmas, 7, 1
Dotani, T., Asai, K., & Wijnands, R. 2000, ApJ, 543, L145
Dubus, G., Hameury, J.-M., & Lasota, J.-P. 2001, A&A, 373, 251
Farouki, R. & Hamaguchi, S. 1993, Phys. Rev. E, 47, 4330
Flowers, E. & Itoh, N. 1981, ApJ, 250, 750
Fontaine, G. & Michaud, G. 1979, ApJ, 231, 826
Fushiki, I. & Lamb, D. Q. 1987, ApJ, 317, 368
Garcia, M. R., McClintock, J. E., Narayan, R., Callanan, P., & Murray, S. S. 2001, ApJ, 553, L47
Gnedin, O. Y., Yakovlev, D. G., & Potekhin, A. Y. 2001, MNRAS, 324, 725
Gudmundsson, E. H., Pethick, C. J., & Epstein, R. I. 1983, ApJ, 272, 286
Haensel, P. & Zdunik, J. L. 1990, A&A, 227, 431
Hameury, J. M., Heyvaerts, J., & Bonazzola, S. 1983, A&A, 121, 259
Heinke, C. O., Grindlay, J. E., Lloyd, D. A., & Edmonds, P. D. 2002, in Neutron Stars in Supernova Remnants, ed. P. O. Slane & B. M. Gaensler, ASP Conference Proceedings, in press (astro-ph/0112127)
Hindmarsh, A. C. 1983, in Scientific Computing: Applications of Mathematics and Computing to the Physical Sciences, ed. R. S. Stepleman et al. (Amsterdam: North-Holland), 55
Itoh, N. & Kohyama, Y. 1993, ApJ, 404, 268
Itoh, N., Kuwashima, F., Ichihashi, K., & Mutoh, H. 1991, ApJ, 382, 636
Itoh, N., Mitake, S., Iyetomi, H., & Ichimaru, S. 1983, ApJ, 273, 774
Itoh, N., Nakagawa, M., & Kohyama, Y. 1985, ApJ, 294, 17
Kaminker, A. D., Haensel, P., & Yakovlev, D. G. 2001, A&A, 373, L17
Koike, O., Hashimoto, M., Arai, K., & Wanajo, S. 1999, A&A, 342, 464
Kong, A. K. H., McClintock, J. E., Garcia, M. R., Murray, S. S., & Barret, D. 2002, ApJ, in press (astro-ph/0111134)
Landau, L. D. & Lifshitz, E. M. 1987, Fluid Mechanics, 2nd edn. (Oxford: Pergamon Press)
Menou, K., Esin, A. A., Narayan, R., Garcia, M. R., Lasota, J. P., & McClintock, J. E. 1999, ApJ, 520, 276
Menou, K. & McClintock, J. E. 2001, ApJ, 557, 304
Narayan, R., Garcia, M. R., & McClintock, J. E. 1997, ApJ, 478, L79
Paquette, C., Pelletier, C., Fontaine, G., & Michaud, G. 1986, ApJS, 61, 177
Pooley, D., Lewin, W. H. G., Verbunt, F., Homer, L., Margon, B., Gaensler, B. M., Kaspi, V. M., Miller, J. M., Fox, D. W., & van der Klis, M. 2002, ApJ, in press (astro-ph/0111212)
Potekhin, A. Y., Baiko, D. A., Haensel, P., & Yakovlev, D. G. 1999, A&A, 346, 345
Potekhin, A. Y. & Chabrier, G. 2000, Phys. Rev. E, 62, 8554
Potekhin, A. Y., Chabrier, G., & Yakovlev, D. G. 1997, A&A, 323, 415
Rutledge, R. E., Bildsten, L., Brown, E. F., Pavlov, G. G., & Zavlin, V. E. 1999, ApJ, 514, 945
—. 2000, ApJ, 529, 985
—. 2001a, ApJ, 559, 1054
—. 2001b, ApJ, 551, 921
—. 2002a, ApJ, submitted
—. 2002b, ApJ, submitted (astro-ph/0105405)

Rutledge, R. E., Bildsten, L., Brown, E. F., Pavlov, G. G., Zavlin, V. E., & Ushomirsky, G. 2001c, ApJ, submitted (astro-ph/0108125)
Sampson, D. H. 1959, ApJ, 129, 734
Sato, K. 1979, Prog. Theor. Physics, 62, 957
Schatz, H., Aprahamian, A., Barnard, V., Bildsten, L., Cumming, A., Ouellette, M., Rauscher, T., Thielemann, F.-K., & Wiescher, M. 2001, Phys. Rev. Lett., 86, 3471
Schatz, H., Aprahamian, A., Goerres, J., Wiescher, M., Rauscher, T., Rembges, J. F., Thielemann, F.-K., Pfeiffer, B., Moller, P., Kratz, K. L., Herndl, H., Brown, B. A., & Rebel, H. 1998, Phys. Rep., 294, 167
Schatz, H., Bildsten, L., Cumming, A., & Wiescher, M. 1999, ApJ, 524, 1014
Spitzer, L. 1962, Physics of Fully Ionized Gases, 2nd edn. (New York: Interscience Publishers)
Stella, L., Campana, S., Mereghetti, S., Ricci, D., & Israel, G. L. 2000, ApJ, 537, L115
Stevenson, D. J. & Salpeter, E. E. 1977, ApJS, 35, 221
Tanaka, S. & Ichimaru, S. 1987, Phys. Rev. A, 35, 4743
Urpin, V. A. & Yakovlev, D. G. 1980, Soviet Ast., 24, 126
van Paradijs, J., Verbunt, F., Shafer, R. A., & Arnaud, K. A. 1987, A&A, 182, 47
Van Wormer, L., Görres, J., Iliadis, C., Wiescher, M., & Thielemann, F.-K. 1994, ApJ, 432, 326
Ventura, J. & Potekhin, A. Y. 2002, in The Neutron Star–Black Hole Connection, ed. C. Kouveliotou, J. Ventura, & E. van den Heuvel, Vol. 567, NATO ASI sec. C (Dordrecht: Kluwer), 393
Wallace, R. K. & Woosley, S. E. 1981, ApJS, 45, 389
Wijnands, R., Kuiper, L., in't Zand, J., Dotani, T., van der Klis, M., & Heise, J. 2002, ApJ, in press (astro-ph/0105421)
Wijnands, R., Miller, J. M., Groot, P. J., Markwardt, C., Lewin, W. H. G., & van der Klis, M. 2001, ApJ, 560, L159
Wijnands, R. & van der Klis, M. 1998, Nature, 394, 344
Yakovlev, D. G., Kaminker, A. D., Gnedin, O. Y., & Haensel, P. 2001, Phys. Rep., 354, 1

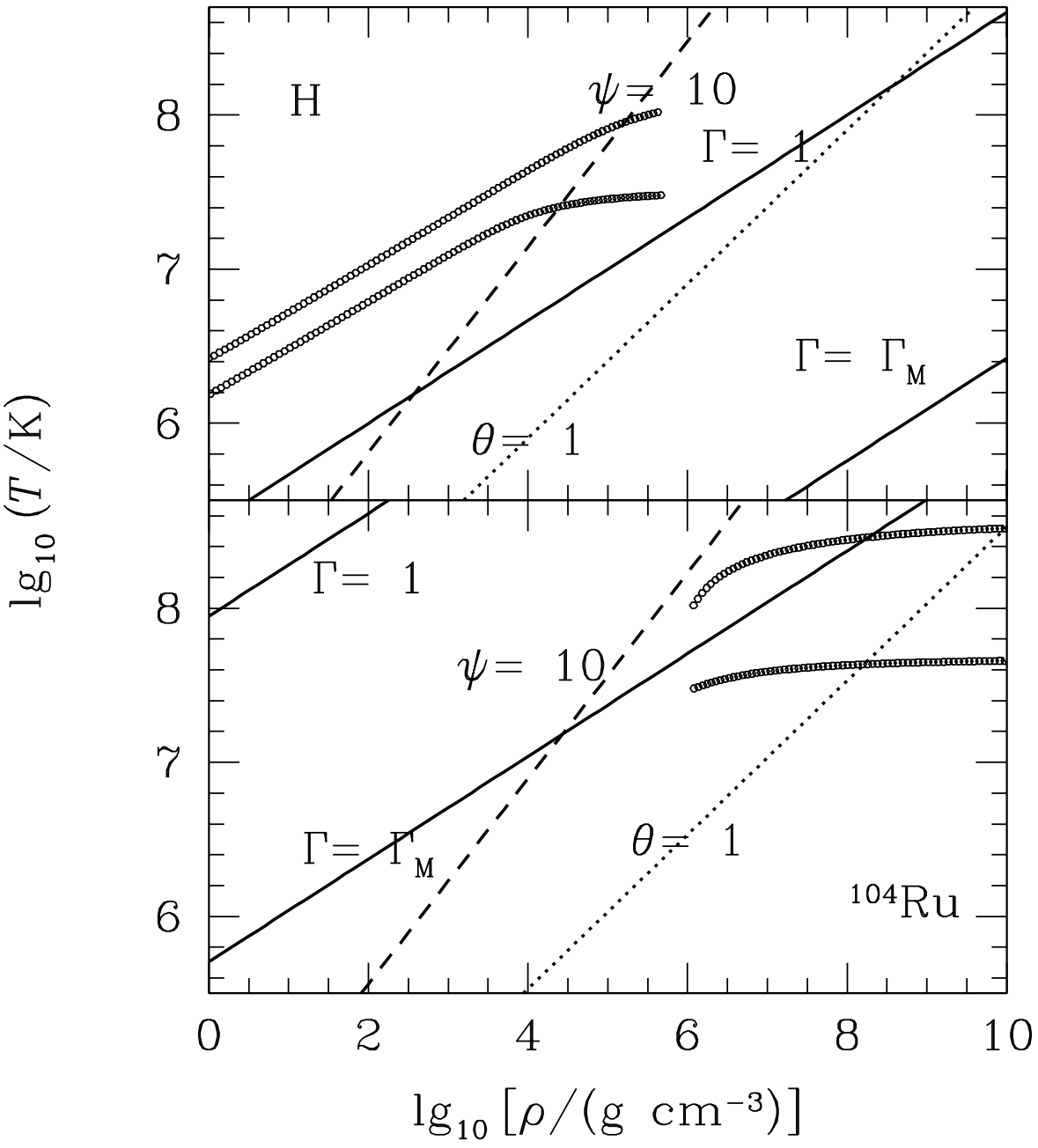

FIG. 1.— Schematic of different physical regimes for a quiescent neutron star envelope. We show the conditions $\Gamma = 1$ and $\Gamma = \Gamma_{\rm M}$ (*solid lines*), $\theta = 1$ (*dotted lines*) and $\psi = 10$ (*dashed lines*), for both H (*top panel*) and ^{104}Ru (*bottom panel*). Circles denote the envelope structure for a two-layer (H over ^{104}Ru) envelope at $T_{\rm eff} = 2.1 \times 10^6$ K (*top curve*) and $T_{\rm eff} = 8.8 \times 10^5$ K (*bottom curve*), as appropriate for Aql X-1 and Cen X-4, respectively (see text).

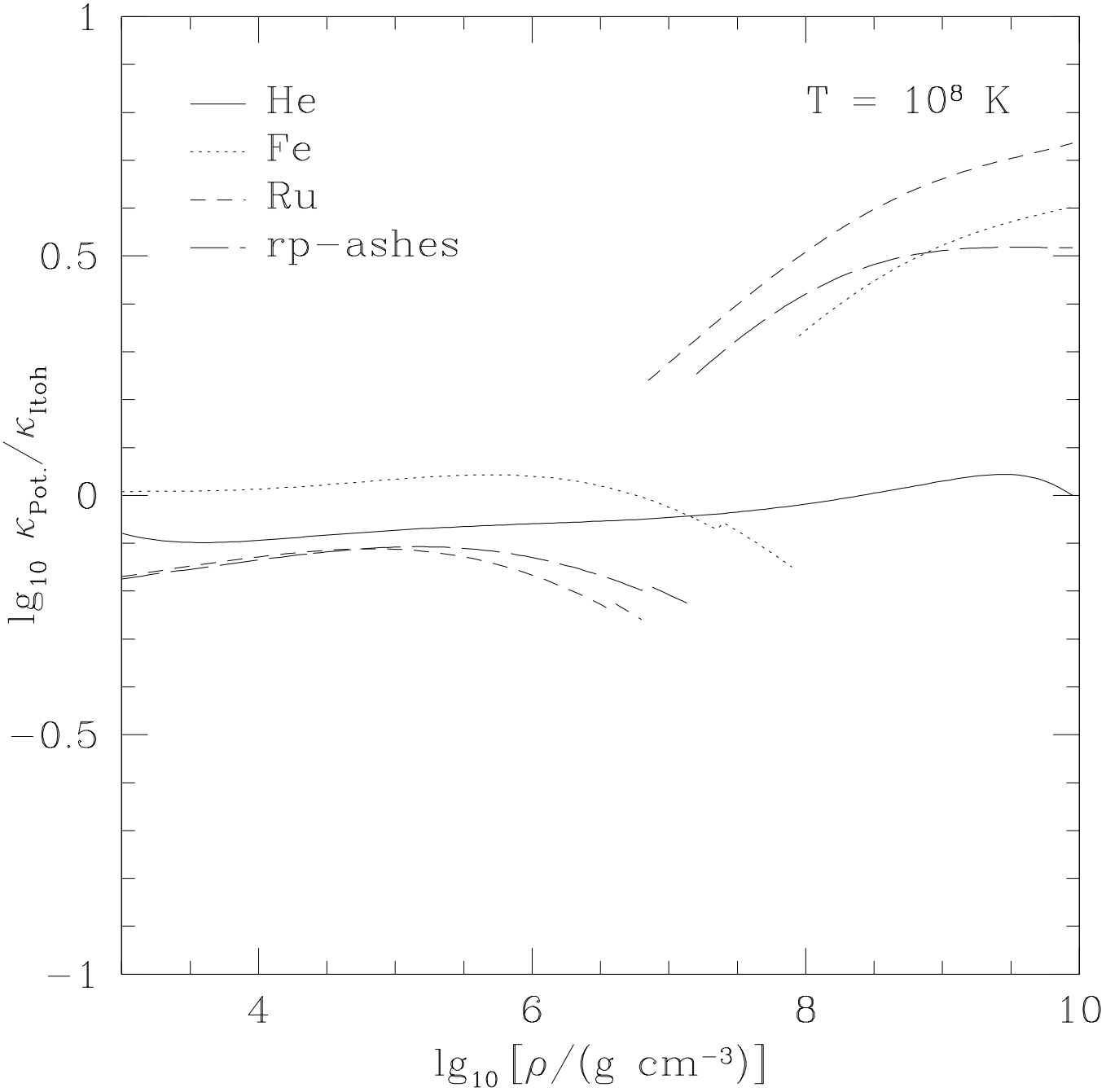

FIG. 2.— Ratio of the conductive opacity as fitted by Potekhin et al. (1999), $\kappa_{\rm Pot.}$, to that fitted by Itoh et al. (1983), $\kappa_{\rm Itoh}$, for various plasma compositions as a function of density at a temperature $T = 10^8$ K. The discontinuities occur at the liquid-solid phase transition. They reflect our choice to use (for the results of Itoh et al. 1983) the liquid metal approximation for $\Gamma < \Gamma_{\rm M}$ and the electron-phonon scattering for $\Gamma \geq \Gamma_{\rm M}$.

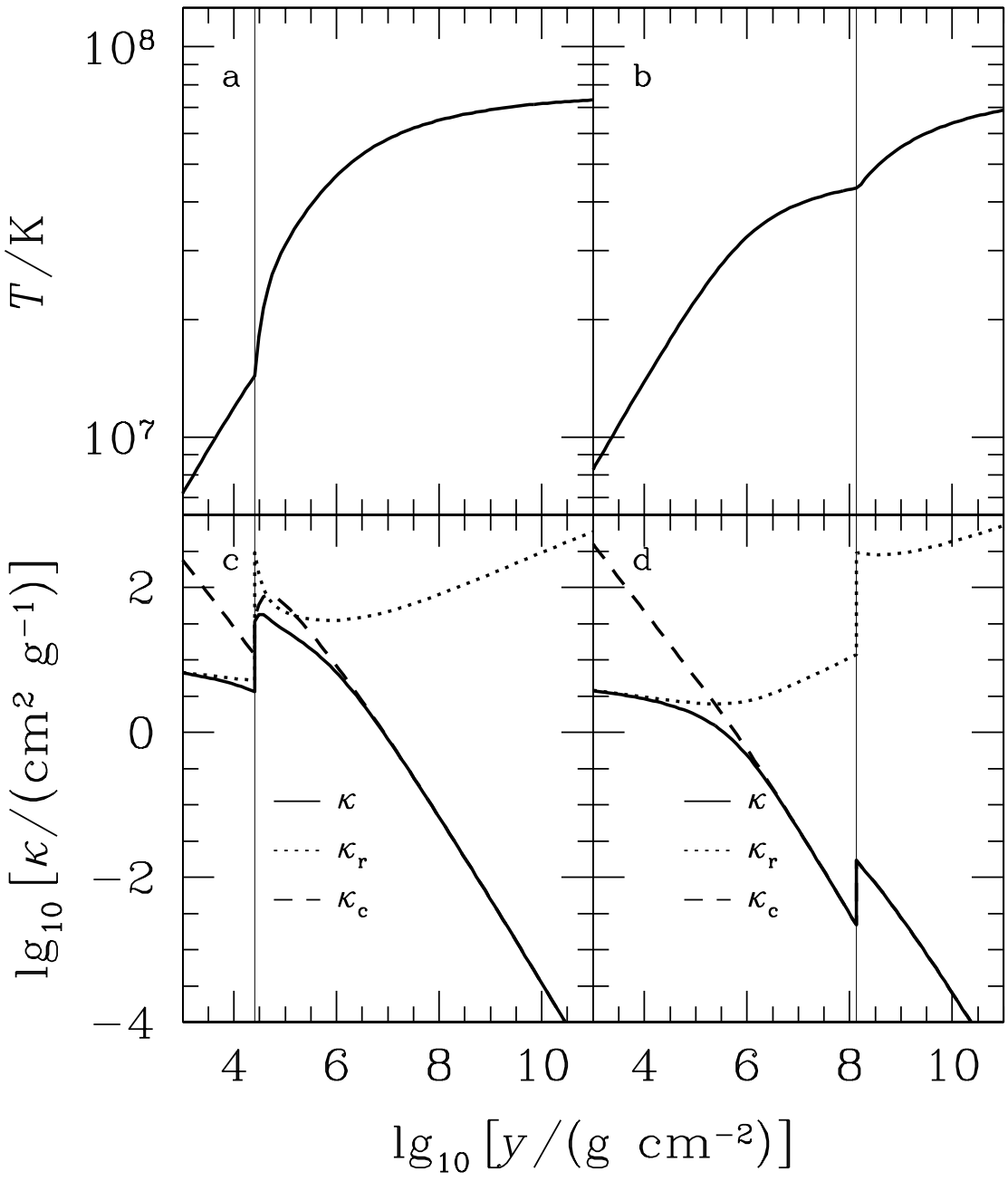

FIG. 3.— Temperature and opacities for a two-layer (H over ^{104}Ru) envelope. The interface between the layers is denoted by the thin solid vertical lines: $y_\mathrm{i} = 2.5 \times 10^4$ g cm^{-2} (*left panels*) and $y_\mathrm{i} = 1.3 \times 10^8$ g cm^{-2} (*right panels*). The top panels depict the temperature; the bottom panels depict the total opacity (*solid lines*), radiative opacity (*dotted lines*), and conductive opacity (*dashed lines*).

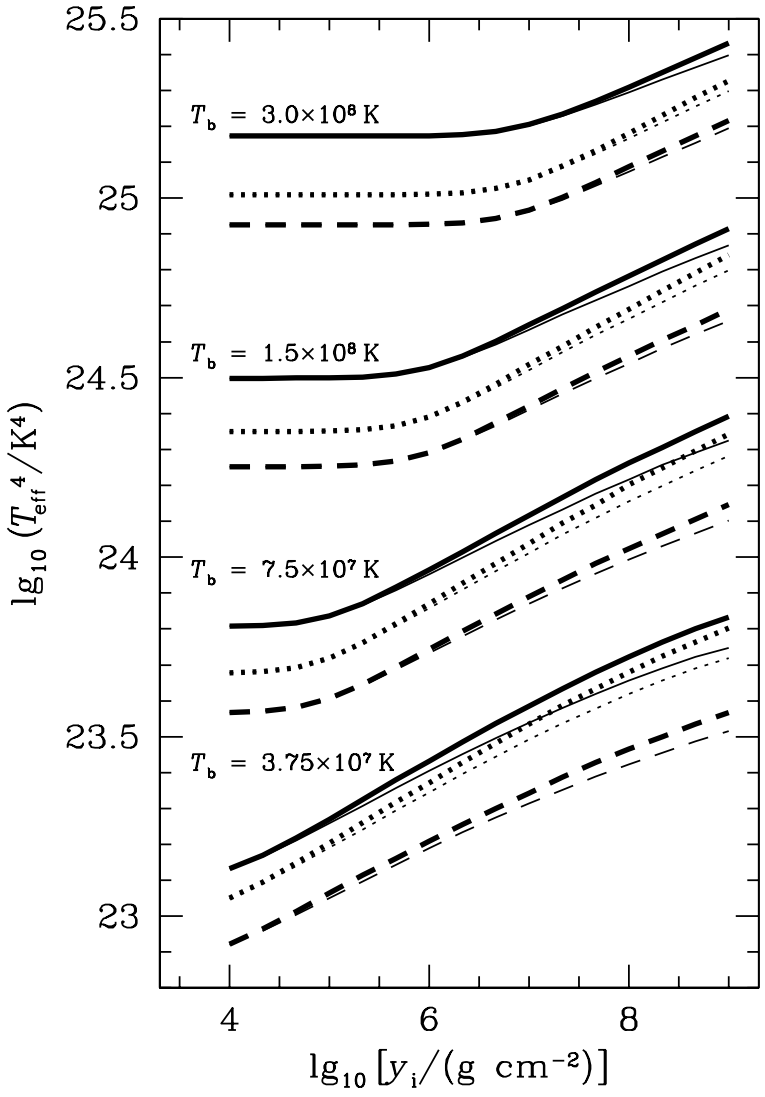

FIG. 4.— Variation of $T_{\rm eff}^4$ with interfacial column $y_{\rm i}$ for a two-layer envelope with a fixed inner boundary temperature $T_{\rm b}$. The top layer is either H (*thin lines*) or ^{4}He (*thick lines*); the bottom layer is either ^{56}Fe (*solid lines*), ^{104}Ru (*dotted lines*), or a very impure ($Q = 233$; K calculated in the mean-ion approximation) mixture from an rp-process burst (*dashed lines*). Each group of curves corresponds to $T_{\rm b} = 3.75 \times 10^7$ K, 7.5×10^7 K, 1.5×10^8 K, and 3.0×10^8 K.

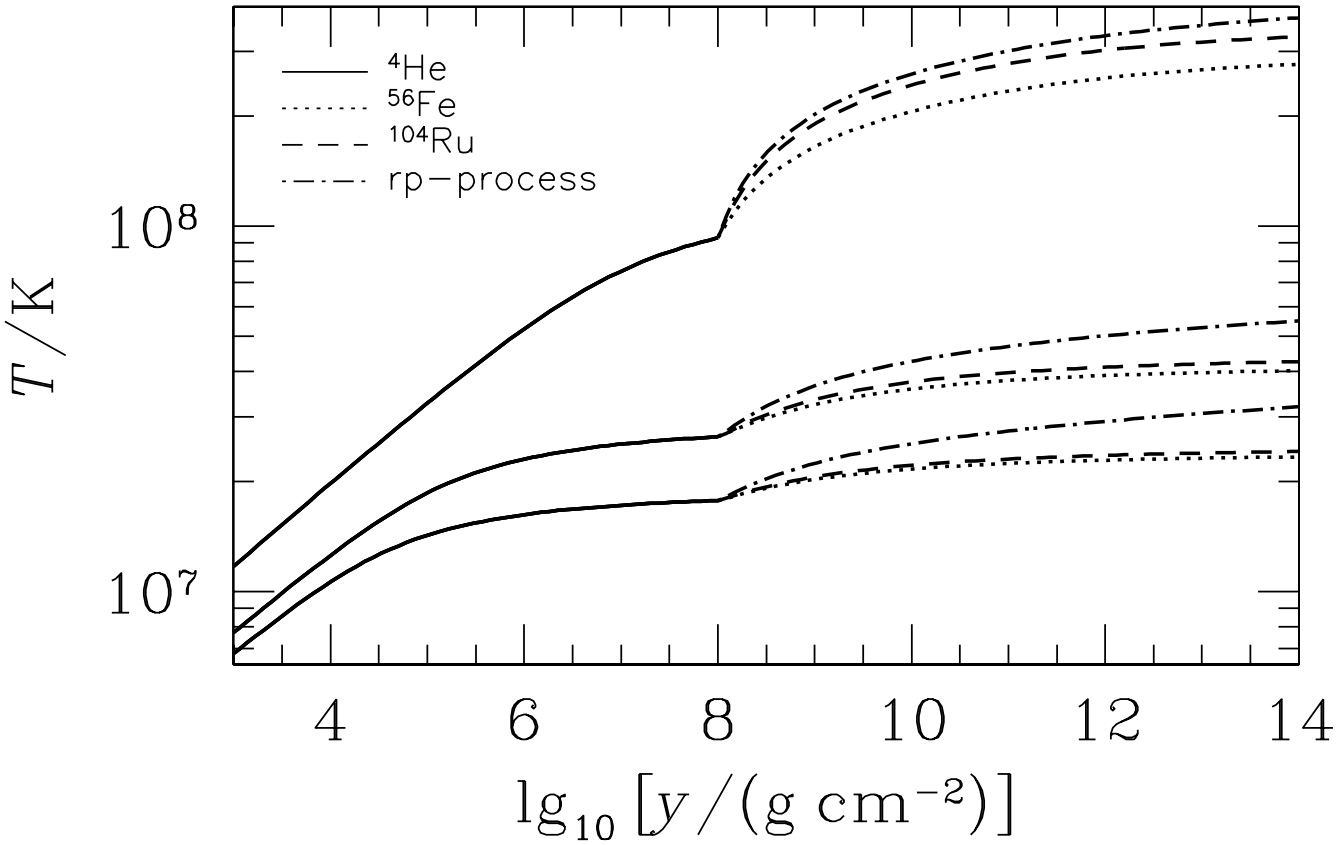

FIG. 5.— Thermal structure of a two-layer neutron star envelope with the interface between the layers at $y_i = 10^8$ g cm^{-2}. The three structures, from top to bottom, are for $T_{\rm eff} = 2.1 \times 10^6$ K (Aql X-1), $T_{\rm eff} = 8.8 \times 10^5$ K (Cen X-4), and $T_{\rm eff} = 6.8 \times 10^5$ K (SAX J1808.4−3658). The composition of the outer layer is ^{4}He (*solid line*). The composition of the inner layer is either ^{56}Fe (*dotted line*), ^{104}Ru (*dashed line*), or rp-process ashes with the mean-ion approximation (eq. [16]) for the conductivity (*dot-dashed line*).